TAIL ROTOR AERODYNAMIC FEATURES RECORDED IN FLIGHT

Lieutenant A D S Ellin Royal Navy
Royal Aerospace Establishment
Bedford, England

Abstract

Following a flight trial with an instrumented tail rotor blade fitted to the RAE flight research Puma, some analysis of the data collected has taken place. The effects of some main rotor and tail fin interactions have become apparent and are illustrated by frequency spectra and polar contour plots of tail rotor pressure coefficients. The problems caused in the analysis of such data by variations in tail rotor blade chordwise velocity are discussed and a possible solution postulated.

Introduction

Although the tail rotor typically consumes between 11% and 14% of the power delivered to a helicopter main gearbox, it can take 30% or more during certain manoeuvres. There are ever increasing demands on performance and handling, especially during either nap-of-earth flight in the battlefield role, or out of wind operations at sea. Hence any reduction in the power consumption of the tail rotor can be of significant benefit, both in the potential increase in power available and the reduction of overall system weight. Any design work to improve tail rotor efficiency requires a detailed knowledge of both tail rotor loadings and the aerodynamic conditions in which the tail rotor operates. In an attempt to improve their accuracy, mathematical models of helicopters are being continually refined to include complex interactional effects. Information on tail rotor loadings and performance are required to guide, extend and validate prediction methods.

When compared with the main rotor, the tail rotor operates in an even more complex aerodynamic environment. The tail rotor airflow can be affected by the wake from the main rotor hub and blades and the influences of the tail fin, the rear fuselage and the ground, the relative proportions of which will vary with aircraft height, attitude, velocity and direction of movement. Before any detailed tail rotor loading calculations can be attempted, a knowledge of this interactional flow is required.

A programme of flight trials to investigate tail rotor aerodynamics has been instigated at RAE Bedford and is proceeding apace. A short series of flights with an instrumented tail rotor blade fitted to the RAE research Puma aircraft has been carried out. The conduct of the trial and the initial stages of the analysis work have been the subject of published papers (Refs 1 & 2). This trial has highlighted certain features in the data and it has become apparent that even more novel approaches to the recording of the data will be required before all ambiguities can be resolved and the features explained.

This paper covers more of the work carried out in the analysis of the data recorded on the Puma, both on the frequency content of the signals and polar plots of individual revolutions. It also looks at the problem of estimating the local chordwise velocity at the blade and a possible solution to this problem.

The Aims and Conduct of the Tail Rotor Flight Research Programme.

The aims of the RAE Bedford tail rotor flight research programme as initially set out (Ref 1) were as follows:

i. To design instrumentation for a standard Puma tail rotor blade to allow pressure distributions along the leading and trailing edges to be recorded in flight.

ii. To perform flight trials without the instrumented blades fitted to determine tail rotor effectiveness and limitations within the aircraft low speed envelope (Phase 1).

iii. To perform a further series of flight trials with the Puma now fitted with the instrumented tail rotor blade to compile a library of tail rotor aerodynamic data, concentrating on those areas of the envelope where Phase 1 showed that tail rotor related handling deficiencies exist (Phase 2).

iv. From the data gathered in Phase 2, to determine tail rotor blade loadings and flow patterns under different flight conditions, thereby improving our knowledge of tail rotor aerodynamics and the resulting effects on performance and flight mechanics.

In the design work on the instrumented tail rotor blade, the experience gained in the use of pressure indicator sensors on main rotor blades for both the Wessex and Puma Helicopters was adapted to meet the slightly differing constraints imposed by the Puma tail rotor blade design. The principles of operation of the pressure indicator sensor, which depends upon the relationship between the output from a single leading edge pressure sensor and local blade incidence and loading, can be found at (Ref 3). Where it had been possible to bury the leading edge sensors in small cavities in the main rotor blade spar, there was insufficient metal in the tail rotor blade spar for this to be possible. Instead, the pressure sensors were mounted on the surface of the blade and covered with a balsa wood and epoxy resin fairing. This fairing extended the chord of the blade forward by 2.7% and has an external shape profiled to NACA 0012 based on the new extended chord length. From a point some 10% chord behind the sensor the fairing is blended back to the original blade profile (fig 1). It was considered that, as far as the sensor was concerned, the blade profile was sufficiently close to NACA 0012 that aerodynamic data from wind tunnel tests of that section could be used in the calculation of incidence and loading with acceptable accuracy. Although only one blade had pressure sensors fitted, 4 additional blades had the fairing fitted so that all 5 blades on the tail rotor presented the same profile. The signals from the sensors were amplified before passing through sliprings into the aircraft PCM recording system (fig 2), the helicopter used for the trial being the RAE flight research Puma (fig 3).

The Phase 1 flight trials were carried out at Bedford in order to highlight those areas of the low speed flight envelope that warranted further in depth investigation with the instrumented blade fitted. During the Phase 1 flying, Responses to control inputs, control margins and handling qualities were studied throughout the low speed envelope, looking in particular for any areas were deficiencies were to be found. It could be said that the Puma was not the ideal helicopter for carrying out such an investigation as it has satisfactory yaw control characteristics but sufficient areas of interest were noted for a full programme of tests with the

instrumented blade to be drawn up. One feature highlighted in the Phase 1 trial was the effect of relatively low wind speeds on aircraft handling, especially during yawing manoeuvres such as spot turns. For this reason a survey of historical meteorological data was carried out to find a suitable airfield in Europe where there was a high probability that low wind conditions would be experienced for the trial duration. Villafranca Airfield in the Po Valley, Northern Italy was the location eventually selected. On completion of shake down flying to test that the instrumented tail rotor was working as planned, the aircraft was flown to Italy and the Phase 2 flying carried out. The test points flown covered steady speed flight at varying sideslip angle and spot turns at both steady yaw rates and constant pedal positions. The transient effects of pedal reversals and finally sidestep acceleration manoeuvres were also investigated. In all some 12 hours flight test were flown over a 2 week period.

On the return flight back to Bedford heavy tail rotor vibration was experienced before leaving Italian airspace and, after rapid diversion to a suitable airfield, it was discovered that the tail rotor slipring assembly had failed. As it had not been possible to inspect any of the recorded data in Italy, it was not until this data was inspected upon return that it was discovered that the sliprings had started to fail part way through the trial. A proportion of the data from the rotating components was lost but sufficient remained for an extensive programme of analysis to be possible. Aircraft body motion and control input information were safely recorded for the entire trial. Unfortunately, one of the flight conditions to be lost was the steady hover outside ground effect but an inside ground effect hover has been recorded. As the RAE Puma was to be retired shortly after this trial, no attempt was made to re-record the lost data with this aircraft.

The Effect of Airflow Velocity Changes on the Pressure Indicator System.

The use of the pressure indicator sensor to determine local blade incidence and loading depends upon a knowledge of the velocity of the airflow at that particular radial location. The velocity of the airflow can be split into components in directions parallel to the blade chord, normal to the blade chord and parallel to the blade span. Changes in the spanwise flow component have little or no effect on the pressure distribution with the exception of areas of supercritical or separated flow. As the relationships upon which the use of the pressure indicator sensor depends are inapplicable under these conditions, spanwise flow can be ignored. Changes in the normal flow component directly affect the local blade incidence and will therefore be detected by the sensor and displayed accordingly. Changes in the chordwise flow component, however, cannot be inferred from the sensor readings. The correlation between leading edge pressure coefficient Cp, and Cn and incidence varies with Mach Number. As the values of Cp and local Mach Number depend on the chordwise velocity, a knowledge of that velocity component is required before any accurate incidence and loading data can be calculated.

In most flight conditions the helicopter main rotor can be assumed to be operating in a uniform airflow. Values of chordwise velocity can therefore be obtained from the aircraft motion and rotor speed. The major disturbances a main rotor blade will experience are the vortices

shed by the preceeding blade(s). The vortex centre-lines are largely parallel to the plane of rotation and the chordwise components of induced velocity are usually small compared to the rotational speed component and, in consequence, neglected. This approximation is valid except during close blade/vortex interaction when, in addition, the leading edge sensor relationships used also break down. The area of the disc affected by vortex induced chordwise velocity changes is proportionately quite small.

The tail rotor presents a different picture in so far as blade/vortex interaction is concerned. During certain flight conditions, a major interaction occurs due to the impingement of main rotor tip vortices on the tail rotor. In these circumstances the main rotor vortex centre-lines are often normal to the plane of tail rotor rotation and, in consequence, induce primarily chordwise velocity changes. Due to the relatively smaller diameter of the tail rotor, these vortices often affect a proportionately larger area of the tail rotor disc than they do of the main rotor.The main rotor downwash can pass over some or all of the tail rotor disc and, depending on the direction of rotation, can have a significant affect on the local chordwise velocity. The local tail rotor blade air velocity is also affected by aircraft motion, blade rotational velocity and the effects of self induced vortex interaction in the same way as the main rotor but, in addition, the tail rotor also experiences the effects of fuselage and fin interactions.

The main rotor induced downwash and vortex effects could be derived from one of the various wake models that exist (Refs 4 & 5) and where no other information exists, this approach must be followed. Due to the complex nature of the interactions mentioned above, it would be preferable that an indication of the magnitude of the chordwise velocity increments were available and a method of providing this is discussed below.

The Measurement of Local Chordwise Velocity

The use of the pressure indicator sensor at the 2% chord position depends on the use of wind tunnel data from the National Physics Laboratory. From this data it is possible to construct look up tables that relate the pressure measured at a point on the chord line for a given Mach Number to the corresponding values of blade normal force coefficient and incidence. The position chosen for the sensor is dictated to a large extent by the sensitivity of the gauge output to incidence and the requirement for reasonable linearity with a well behaved reaction to change in Mach Number.

The principle of a possible method for determining chordwise velocity is now described. If 2 pressure sensors are mounted on the chord line well ahead of the the trailing edge they will respond to a given incidence and normal loading change at constant Mach Number with different pressure changes. Similarly, at constant incidence, they will respond differently to a change in Mach Number. For each sensor, lines of constant pressure can be plotted against incidence and Mach Number. If 2 such plots are compared it is possible, by careful selection of the sensor positions, to derive unique values for Mach Number and incidence for each pair of pressure values from the 2 sensors (fig 4). The Mach Number thus obtained can be converted to a velocity and used in the calculation of the pressure coefficient for entry to the 2% chord lookup tables in the normal way.

In choosing the position of the 2 sensors the 2% chord position fulfills the criterion for one of the 2 positions, namely high sensitivity to incidence. For the second sensor the sensitivity must be significantly less in order to provide a good intercept but not so low as to make the measurements overly susceptible to recording errors. The requirements for a good intercept and the reduction of compressibility effects dictate that the second sensor be placed further aft along the chord at approximately 40-50%. A suitable fairing must be produced to cover both sensors without significantly altering the blade section.

It can therefore be seen that it is, in principle, possible to derive values for local chordwise velocity under steady flow conditions by the careful placement of an additional sensor. In order to investigate whether this will work in practice in the unsteady flow field of a rotor it is intended to study main rotor data where a full chordwise array was recorded. If practice follows theory, correlation between 2 suitable sensor readings should result in a value for the blade chordwise velocity component. This, of course, should be equal to the sum of the standard rotational and forward speed components for the majority of azimuthal positions with small excursions caused by the blade/tip vortex interaction. If, however, the results of this investigation are encouraging it is intended that the instrumented tail rotor intended for our Lynx after conversion to Mk7 standard be fitted with the extra row of sensors.

It is intended to fly the RAE Lynx at its current Mk5 standard prior to conversion to Mk7, a major part of the modification being the reversal of the tail rotor direction of rotation from top-blade-forward to top-blade-aft. If it were not possible to allow for the effects of the main rotor downwash and hub wake on the tail rotor blade velocity, the value of a comparative trial between the 2 systems would be reduced.

Analysis of Puma Instrumented Tail Rotor Data

As previously stated the Puma instrumented tail rotor blade was fitted with a row of pressure sensors at 2% and a row at 95% chord. Direct measurement of the air velocity is therefore not possible. Unless the position and strength of the main rotor wake can be calculated, it's effect on the tail rotor airflow can not be included. It must be said, however, that the velocities in the main rotor wake are an order of magnitude less than those induced by the tail rotor rotation, especially at the blade tip. Until the effect of this additional flow is quantified, calculation of tail rotor loadings can, at best, be considered suspect and for this reason no attempt has been made to convert the results to incidence and Cn variation using look-up tables.

There is nevertheless still much to be learned from a study of the data. The raw pressures read from the sensors have been converted to coefficients of pressure taking the velocity from the blade rotational speed and the component of aircraft translational movement. Although it would be incorrect to take any quantitative measurements from the data in this form, it still provides qualitative information on the effects of the various interactions occurring at the tail rotor.

When carrying out analysis of main rotor data in a steady flight condition, it is normally sufficient to study only 1 revolution of data as the effects

observed are repeatable, revolution to revolution. For the tail rotor this is not the case. The relative gearing between the main and tail rotors on the Puma is such that the effect of the main rotor vortex interaction with the tail rotor is approximately repeatable every 193 tail rotor revolutions. A large number of revolutions need to be studied in order to build up as complete a picture as possible. When recording the data during the flight trial, each flight condition was held for a minimum of 6 seconds and this has been chosen as the standard length of event to be analysed, each such event containing about 127 tail rotor revolutions.

It is possible to look at each event in 2 ways. Frequency analysis of the complete event will show the dominant influences on the tail rotor and their relative importance. Polar plots of single revolutions will show the areas of the disc where these effects are taking place and their exact nature. Although the polar plots are more revealing, the 2 techniques are complementary with the frequency plots showing cause and the polar plots effect.

Frequency Analysis of Complete Events.

In order to obtain acceptable azimuthal resolution for the production of accurate polar contour plots, it was necessary to sample the tail rotor data at 4096 samples per second. This sampling rate is more than adequate for frequency analysis up to the 10th tail rotor harmonic (10T). The analysis will, however, only reveal that an influence of a certain frequency has affected some part of the tail rotor disc and can not isolate where on the disc it occurred. To do this, study of one or many polar contour plots of the individual revolutions is required. Reading between the 2 techniques allows the full picture to be established.

(Fig 5) shows the frequency content of the pressure coefficient derived from the 84% radius leading edge sensor during 20Kts forward flight outside ground effect. The predominant features are the harmonics of the tail rotor rotational frequency. This 1T frequency is a result of those effects that are stationary on the disc and do not vary significantly from one revolution to the next. Such features are the tail rotor tip vortex interference and tail fin interference effects. In nearly all cases the 1st harmonic predominates with the remainder decreasing in amplitude in order. The effect of interference with the main rotor wake can be seen as much smaller pulses either side of each tail rotor harmonic. The 1st of these occurs at the main rotor blade passing frequency with the remainder spaced (1T - 4R) either side of the tail rotor harmonics. These main rotor associated peaks are only present when the main rotor wake passes over or close to the tail rotor and even then are sometimes buried in the signal background noise. The other feature of note is the low frequency peak at about 1 Hz. This is evidence of the control activity being applied by the pilot to maintain a steady flight condition.

(Fig 6) shows the signal from the same sensor but this time with the aircraft flying at 25 Kts outside ground effect with a sideslip angle of Red 065. In this event the even tail rotor harmonics (2T, 4T etc.) are stronger than the preceeding odd ones (1T, 3T etc.). This only occurs with relative winds in the region of 050 to 120 either side of the nose; the effect being more dominant with Red winds ie. those from port. This is thought to be evidence of

increased interference round the tail fin though the exact mechanism is unknown. The main rotor blade passing frequency (4R) effects are not visible but a very strong peak at twice this frequency (8R) is present. This 8R peak can only be found with relative winds of about Red 060 and during the event shown in (fig 7), where this effect is very strong, the pilot was experiencing 'tail rotor buzz'. This 8R frequency is thought to be caused by the tip vortex shed from the edge of the main rotor disc passing either side of the tail fin prior to affecting the tail rotor.

In addition to the variation in individual sensor signal content with flight condition, the signals for the various sensors along the blade can differ. A summary of the main features noted is as follows:

i. Relative winds from ahead to Red 045 (fig 8).

The tail rotor harmonics are graded such that the peak heights diminish with increasing order of harmonic. The 1st harmonic is strong at the tip as evidence of the tip loading peak. It is weaker in the middle of the blade but becomes stronger again towards the root. At the higher speeds the fin interference effect region is only visible at the root of the blade and this forms evidence of it. Main rotor blade passing frequency peaks can be seen either side of all tail rotor harmonics but are not easily visible in all cases. Little control activity is present indicating that the flight conditions are easy to hold.

ii. Relative winds between Red 045 and Red 135 (fig 9).

Here the 2nd harmonic tail rotor harmonic is stronger than the 1st for reasons given above. The effects of the main rotor blade passing frequency are not present after Red 070. About Red 060 at higher speed a strong 8R peak is present and tail rotor buzz can be experienced. More noticeable control activity is present, especially around Red 060; this possibly being required to counter the increased interference and turbulence in the flow round the fin.

iii. Relative winds between Red 135 and astern (fig 10).

Only tail rotor harmonics are present with the 1st harmonic predominating. The effects of the tip loading peak can be seen in the strength of the 1st harmonic at the tip; in these instances the tip loading peak segment is at the rear of the disc. Few events were recorded in this region of the flight envelope due to aircraft flight clearance limitations.

iv. Green relative winds (fig 11).

The frequency content of the signal is almost universally weak with tail rotor harmonics above 3T being barely discernable. At speeds less than 20 kts with relative winds about green 060 the second harmonic predominates but this effect is reversed as the speed rises. Higher control activity is also evident in these cases. The low signal content is caused by the tail rotor being off-loaded by the airflow acting on the side of the fuselage and the reduction in the fin interference effects. Main rotor blade passing frequency is visible round to Green 070 at similar strengths to those in the Red wind cases observed.

Polar Plots of Individual Revolutions.

Display Formats. Contour plots of individual revolutions have been drawn to common formats. These are as follows:

i. In (fig 12) the main rotor disc is shown with the aircraft nose pointing up the page; 0° azimuth being aft over the tail. The main rotor of the Puma revolves clockwise when viewed from above, the opposite direction to that of most British and American helicopters. In order to improve commonality of display the rotor has been drawn rotating anticlockwise or as viewed from below.

ii. In (fig 13 et seq) the tail rotor disc is illustrated with the aircraft nose pointing to the left of the page; 0 degree azimuth being with the blade in the aft horizontal position. The puma tail rotor is mounted on the starboard side of the aircraft so the plots show the view looking through the tail fin at the rotor.

For both the main and tail rotors, the contours show lines of constant negative leading edge Cp with the velocity term in the coefficient based on blade rotational velocity and aircraft translation as previously discussed. This display format has been selected as the more negative the Cp, the higher the blade incidence and loading. The plots are produced by looking sequentially at a series of outputs from the sensors on the one instrumented blade per rotor and thus do not produce an instantaneous snapshot of the pressure distribution but a sweep around the disc. This must be remembered when any analysis of the data is carried out and the skewing effects taken into account. For a condition where the pressure distribution remains constant this skewing is not apparent but becomes more significant in unsteady conditions where a discontinuity in the contours is observed.

(Fig 12) shows a polar contour plot of one revolution of the main rotor in the hover outside ground effect. Three main features can be noticed in this plot. The most obvious is the almost axisymetric loading peak just inboard of the blade tip. This is caused by the blade meeting the tip vortex shed by the preceeding blade which reduces the normal flow component at the tip but increases it by a similar amount just inboard. The next feature is the uniform low loading towards the centre of the disc, the striations evident in the plot being caused by the plotting routine. Finally, in the quadrant between 290 and 030 degrees azimuth, the tip loading peak disappears. If the aircraft was translating laterally in any direction the tip vortex interference effect would be displaced towards the opposite side of the disc and, as speed built up, would miss the edge of the disc altogether giving the effect shown here. Although this was initially thought to be the cause in the hover case shown here, the aircraft was, in fact, in a near perfect hover and this effect has since been discounted. For all the perfect hovers observed this gap in the tip loading peak is in the same region of the disc and is now considered to be caused by the influence of the flow through the tail rotor.

(Fig 13) shows a polar contour plot for one revolution of the tail rotor in the hover inside ground effect and displays many similarities with that of the main rotor just described. The central area of uniform low loading and the tip loading peak are both present as is the gap in the loading peak, this time present between 160 and 240 degrees azimuth and caused by the influence of the main rotor. The main rotor wake does not pass across the tail rotor disc in this flight condition but is close enough to influence it as can be seen from study of the frequency content of the signals. Another

feature shown on the plot is the effect of the fin interference on the tail rotor evident between 100 and 150 degrees azimuth. The blocking action of the fin causes a change in the inflow angle resulting in the rise in loading shown.

As the aircraft starts moving forwards at 10 kts as shown in (fig 14), the tip loading peak is missing at the back of the disc as expected. The fin interference effect region has also moved slightly further aft. The main difference between this event and the hover case is that the main rotor wake is now cutting across the tail rotor disc instead of passing down ahead of it. It has proved possible to observe the effect of a tip vortex shed by a main rotor blade on the tail rotor. In (fig 14 A and B) the tail rotor tip loading peak appears to be pushed inboard in the segment indicated and some 'necking' occurs. The position of the main rotor whilst the instrumented tail rotor blade is at 180 degrees azimuth is shown in the small plot to the left of each figure. As the main rotor rotates, the section of the tail rotor tip vortex ring isolated by the 'necking' observed above separates from the rest of the ring (fig 14C) and then moves downwards (fig 14D and E) until it merges with the fin interference effect (fig 14F). As it initially separates, this segment of the tip loading peak is very intense, the variation in Cp over the peak being over 60% of the total range. This main rotor interference effect cannot be seen as it leaves the disc as this occurs within the fin interference effect region.

(Figs 15 and 16) show similar effects in 20 kts and 30 kts forward flight respectively. The tip loading peak is progressively covering a smaller arc and moving further inboard. The fin interference effect has markedly reduced and moved aft as the forward component of flow through the tail rotor has increased. The passage of the main rotor tip vortex effect has again been highlighted and, as would be expected, moves further up the disc with increasing forward speed. For some reason, which is not as yet understood, although it is possible to follow the vortex effect as it crosses the central rotor cutout it is not possible to follow it completely from one edge of the disc to the other. In an attempt to see the movement of this main rotor vortex effect more clearly a method for studying this motion dynamically on video has been devised as described in (Ref 2). Even with this facility it has not proved possible to follow the main rotor tip vortex effect right across the tail rotor disc.

(Fig 17) shows a prediction of the paths of the main rotor tip vortices at these forward speeds using the method outlined in (Refs 6 and 7). No account has been taken of the aft entrainment of the main rotor wake detailed at (Refs 8 and 9) which would tend to move the paths shown rearwards in the vicinity of the tail rotor. If this effect was to be included, the vortex paths would not be far removed from those seen in (Figs 14,15 and 16).

Turning now to sideways flight, (Fig 18) shows polar plots of individual tail rotor revolutions for flight at 10, 20 and 30 kts with sideslip angles approaching 90 degrees in both directions. The main rotor wake does not impinge on the tail rotor in these flight conditions and the loading patterns illustrated does not significantly change from revolution to revolution. For pure sideways flight the tip loading peak should be almost axisymetric as is the case for the hover. Where portions of this peak are missing in the events illustrated some forward or rearward velocity

component is present.

As the aircraft moves to the right the airflow acting on the side of the fuselage and fin counteracts the main rotor torque reaction thus offloading the tail rotor and reducing the rotor induced velocity. This induced velocity is slightly increased however by the sideways motion of the aircraft. As the inflow velocity is reduced, the effect of the tail fin on the inflow angle also decreases and with it the strength of the region of increased loading behind the fin. At 30 kts there is no evidence of this fin interference at all. As the tail rotor blades are offloaded, the strength of the tip vortex and thus its effect on the following blade is diminished. With the aircraft moving to the left all these effects are reversed resulting in the significant changes in loading patterns between left and right sideways flight shown.

Conclusions and Future Developments

A series of flight tests have been carried out using a Puma to investigate helicopter yaw control at low speed and detailed tail rotor aerodynamics. Despite a progressive instrumentation failure during the trial, much informative and useful data was obtained as described and discussed in the present paper. The principle findings are summarized below:

i. The use of leading edge pressure sensors on the tail rotor has enabled the identification of various fuselage, fin and main rotor interference effects including those from discrete main rotor tip vortices. The removal of a segment of the main rotor tip loading peak by the influence of the tail rotor is included from previous main rotor test results and compared with a similar effect observed on the tail rotor.

ii. The tail rotor results have not been fully reduced to incidence and normal force coefficient form because of the likely presence of chordwise components in the interference velocities, the strength of which are currently unknown. The use of a further indicator sensor to determine the magnitude of these effects is discussed.

iii. The study of the frequency content of the periodic interference phenomena has proved useful in the identification of their various sources in the complex tail rotor environment.

iv. A comprehensively instrumented Lynx helicopter has now taken over from the Puma as a test vehicle in aero-mechanic research at RAE. It is planned to enlarge the tail rotor aerodynamic data base using extended tail rotor instrumentation on this aircraft including the use of additional sensors to identify chordwise velocity.

v. The practicality of using a second sensor in this manner will be examined using data from complete chordwise pressure distributions previously measured on the Puma.

vi. It is hoped that information on the effects of tail rotor direction of rotation can be gathered by conducting a comparative trial of tail rotor performance and aerodynamics before and after conversion of the Lynx from Mk5 to Mk7 standard.

References

1. S F Baldwin and C S Handley, "Flight tests to explore tail rotor limitations in the low speed envelope", 14th European Rotorcraft forum, 1988, paper 111

2. A D S Ellin, "Flight measurements illustrating key features of tail rotor loading distribution", RAES Conference on helicopter yaw control concepts, Feb 1990

3. P Brotherhood and M J Riley, "Flight experiments on aerodynamic features affecting helicopter blade design", 3rd European Rotorcraft Forum, 1977

4. T R Quackenbush et al, "High resolution flow field prediction for tail rotor aeroacoustics", 45th AHS Forum, 1989, page 99

5. T S Beddoes, "A wake model for high resolution airloads", US Army/AHS Conference on rotorcraft basic research, Feb 1985

6. A J Landgrebe, "The wake geometry of a hovering helicopter rotor and its influence on rotor performance", Journal of AHS, 1972, Vol 17, No 4 pages 3-15

7. J D Kocurek et al, "Hover performance methodology at Bell Helicopter Textron', 36th AHS Forum, 1980, paper 3

8. R R Lynn et al, "Tail rotor design Part 1: Aerodynamics", Journal of AHS, 1970, Vol 15, No 4 pages 2-15

9. A Brocklehurst, "Main rotor/tail rotor interactions near hover", Westlands research memorandum R.M. 535, 1986

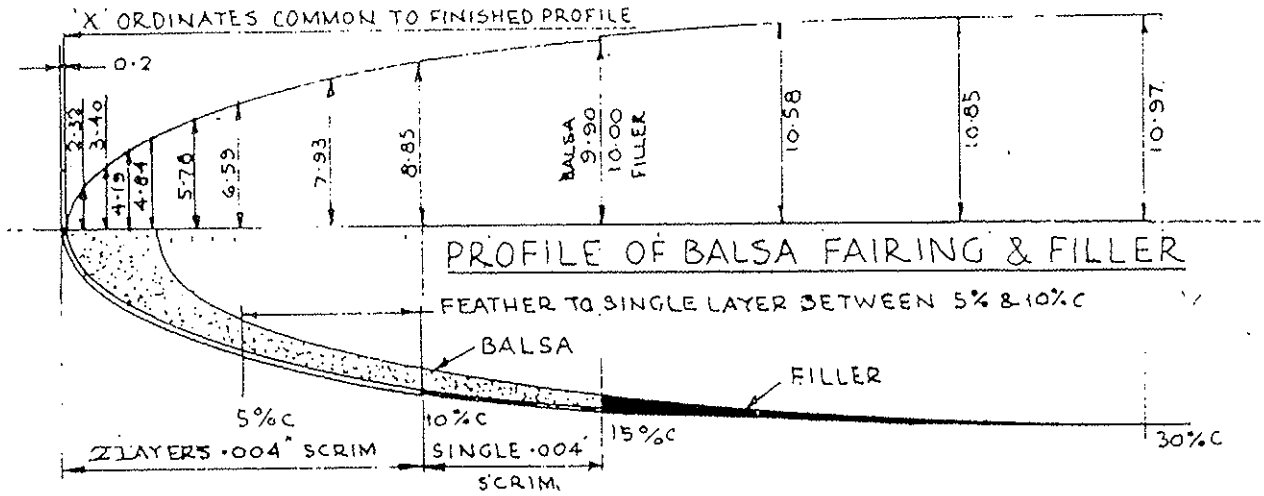

Fig 1 Cross section of blade leading edge fairing

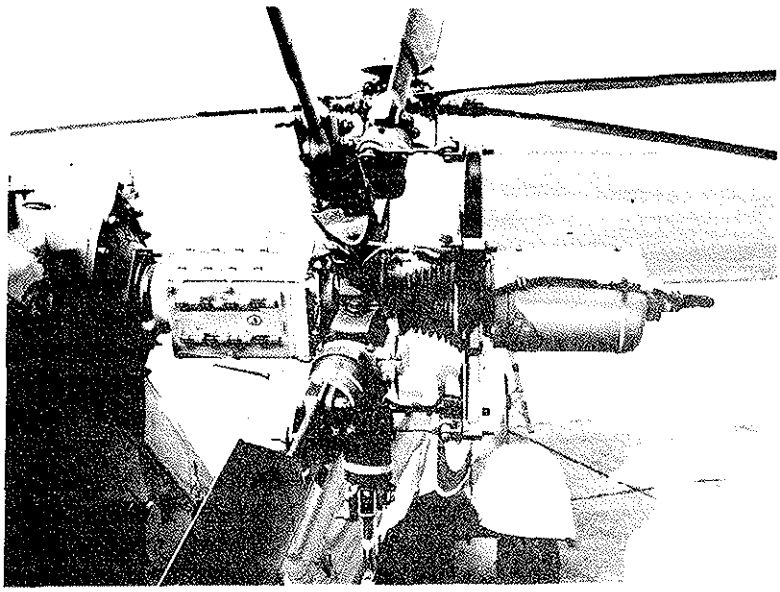

Fig 2 Instrumented tail rotor assembly

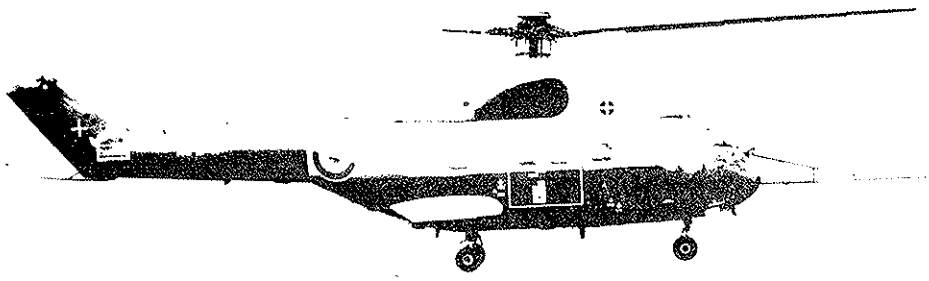

Fig 3 RAE Research Puma XW241

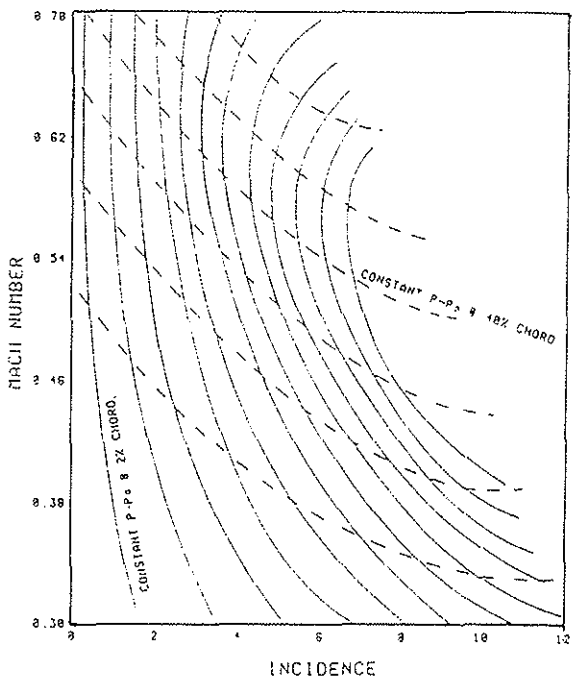

Fig 4 Lines of constant pressure at 2% and 40% chord

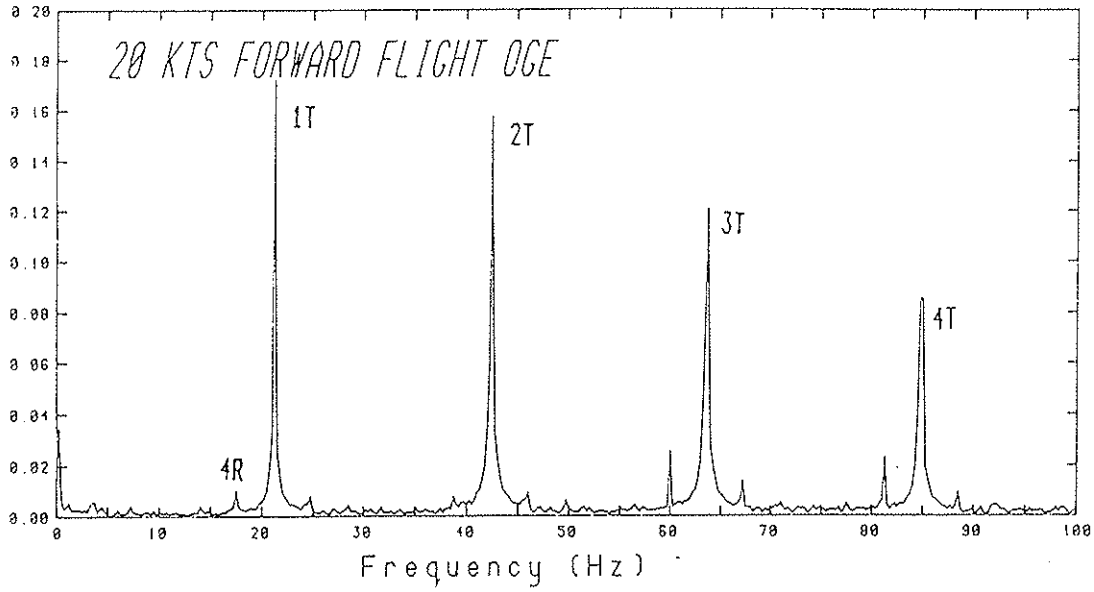

Fig 5 Frequency content at 84% sensor

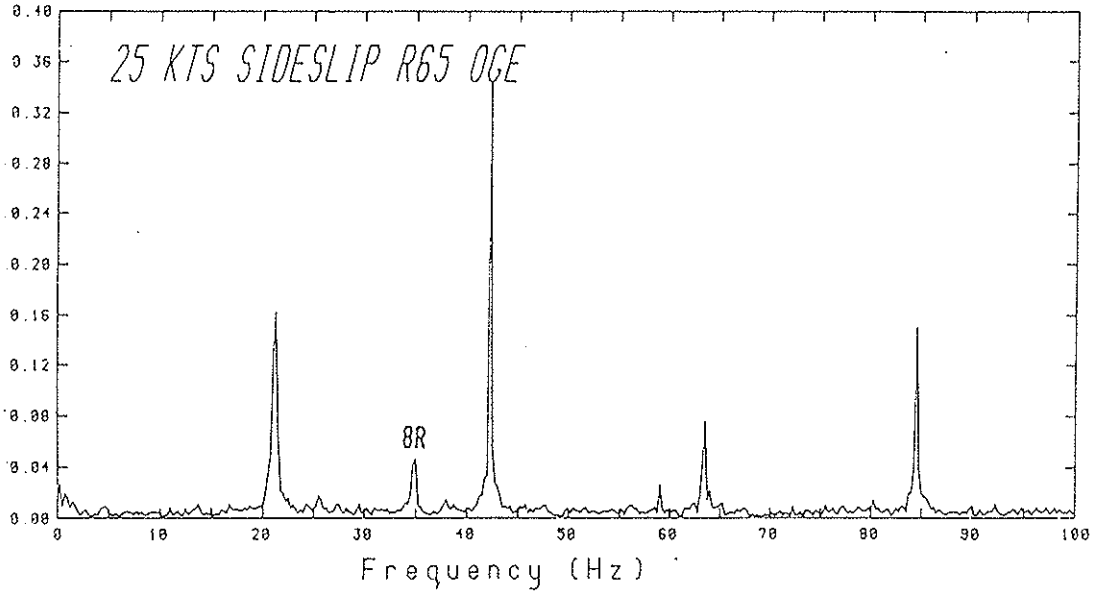

Fig 6 Frequency content at 84% sensor

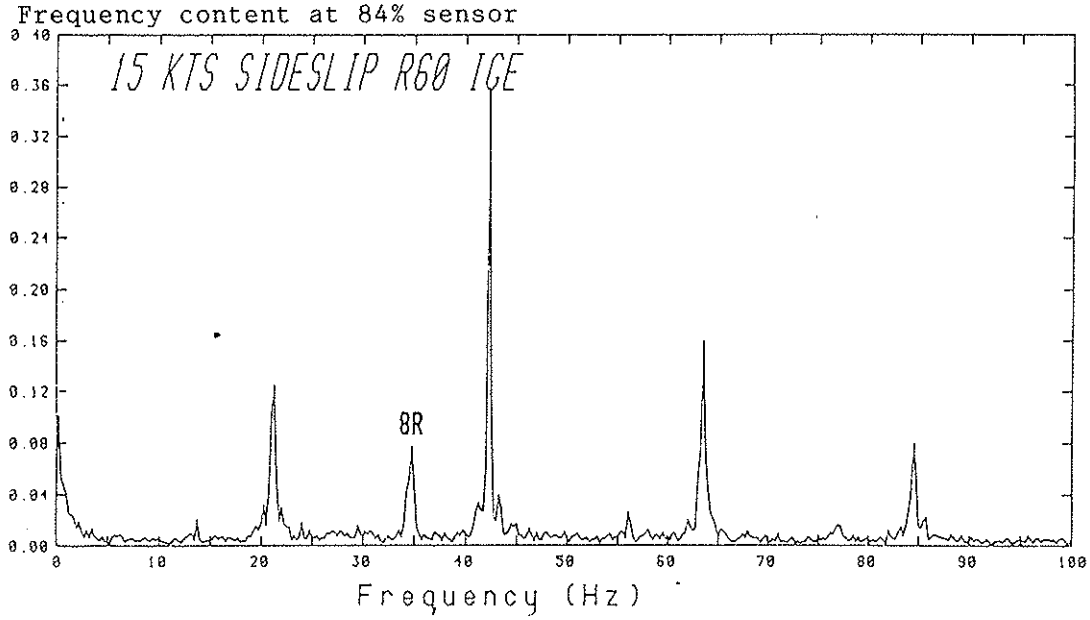

Fig 7 Frequency content at 84% sensor

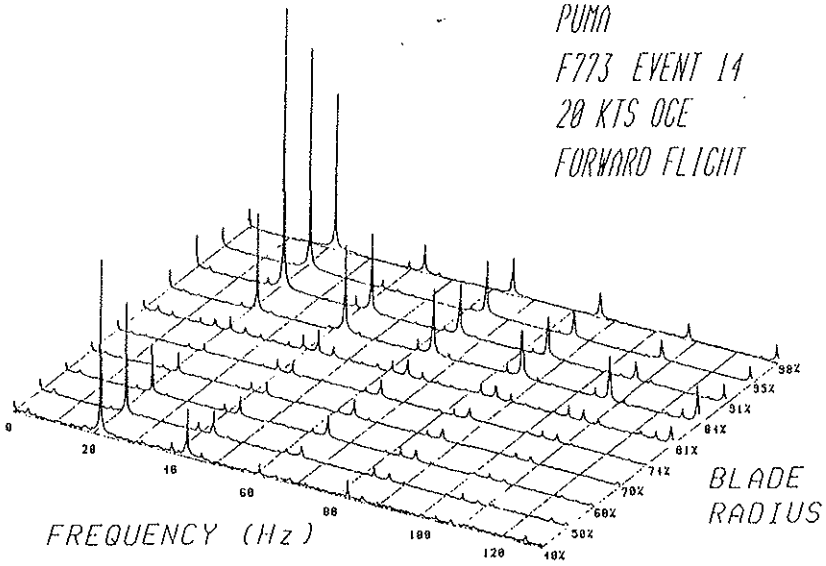

Fig 8 Blade frequency carpet plot

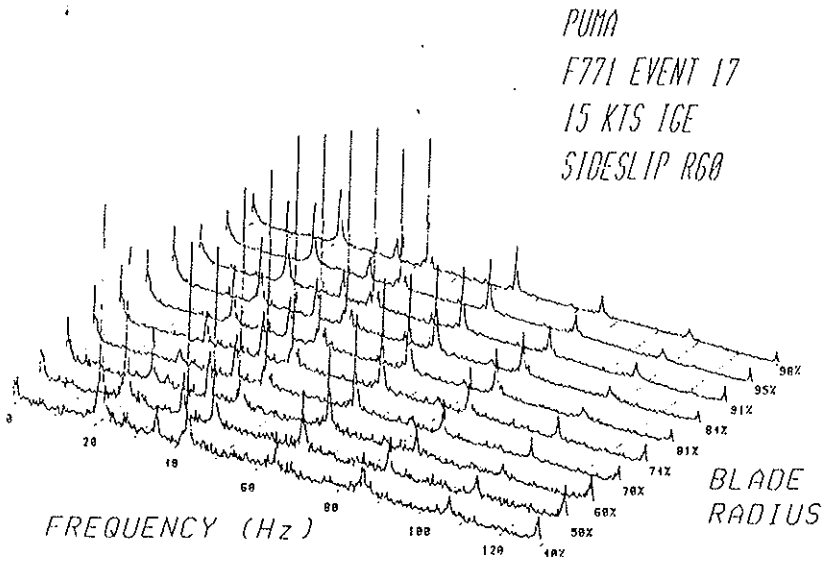

Fig 9 Blade frequency carpet plot

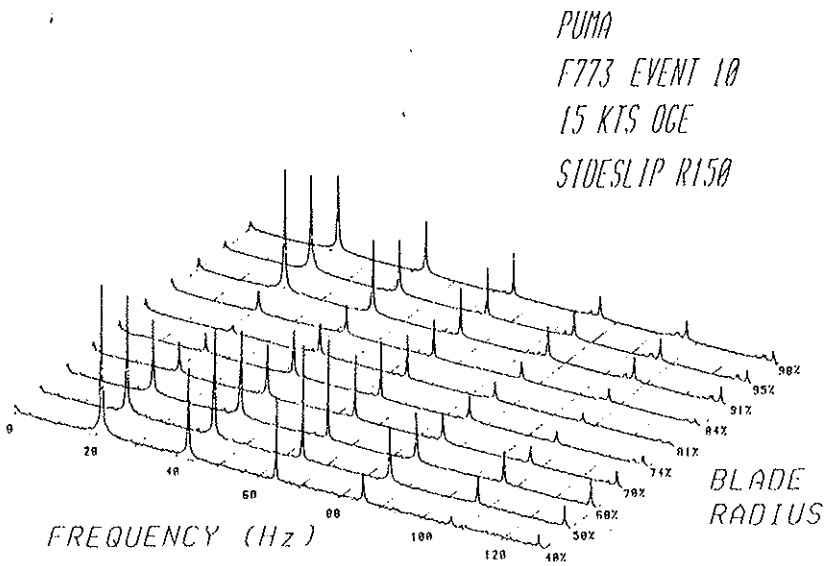

Fig 10 Blade frequency carpet plot

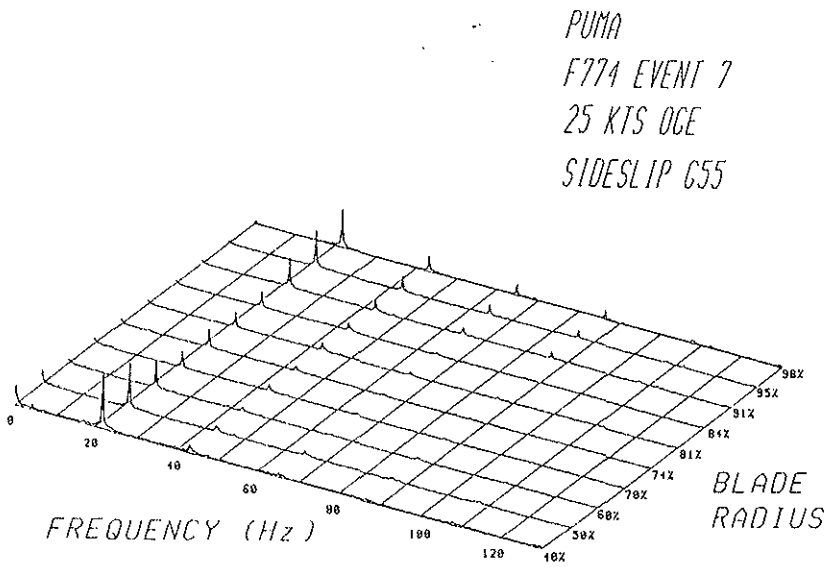

Fig 11 Blade frequency carpet plot

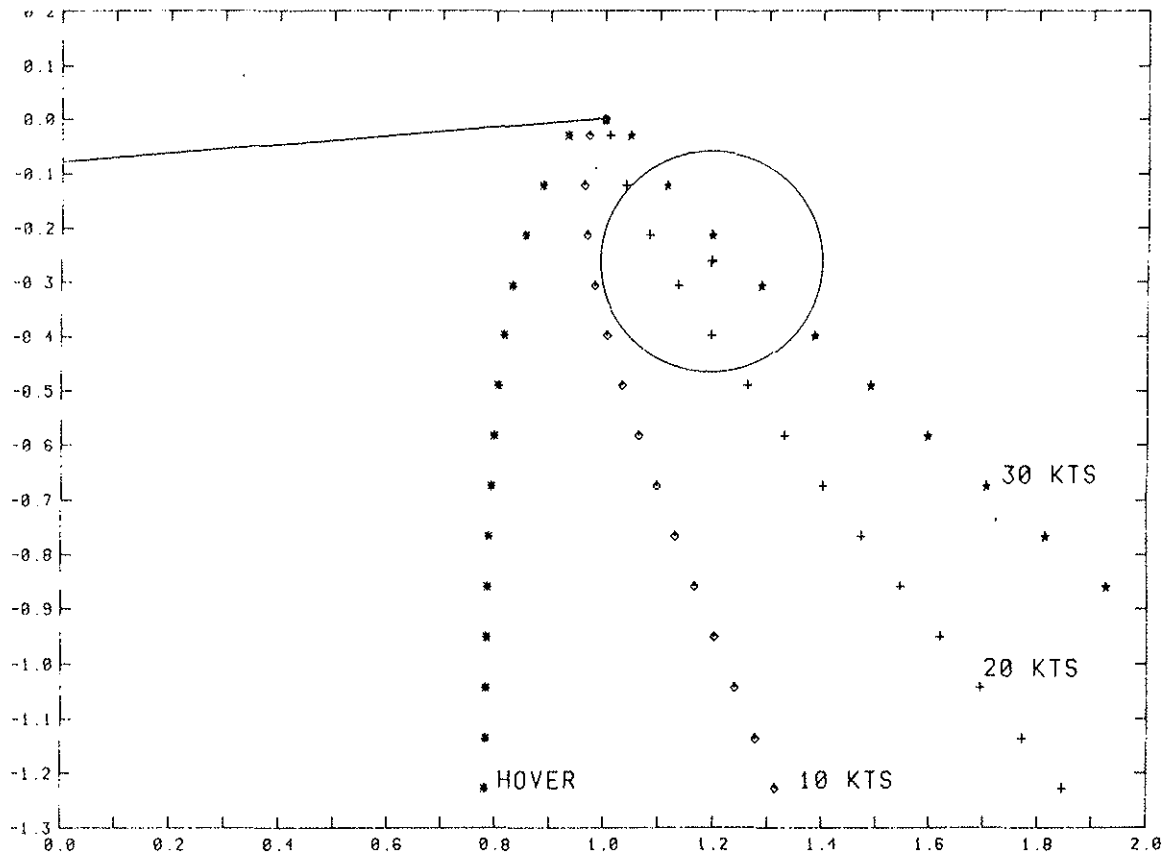

Fig 17 Prediction of main rotor tip vortex paths

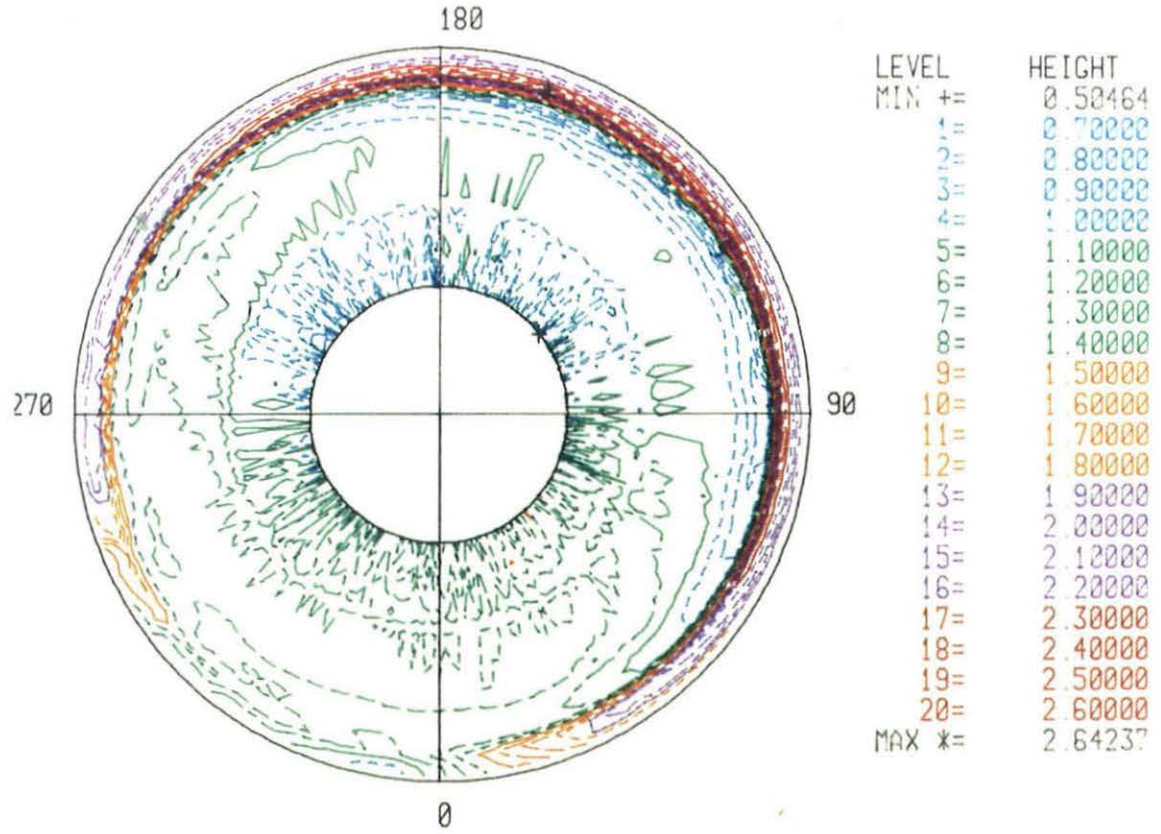

Fig 12. Polar plot of main rotor negative Cp in hover

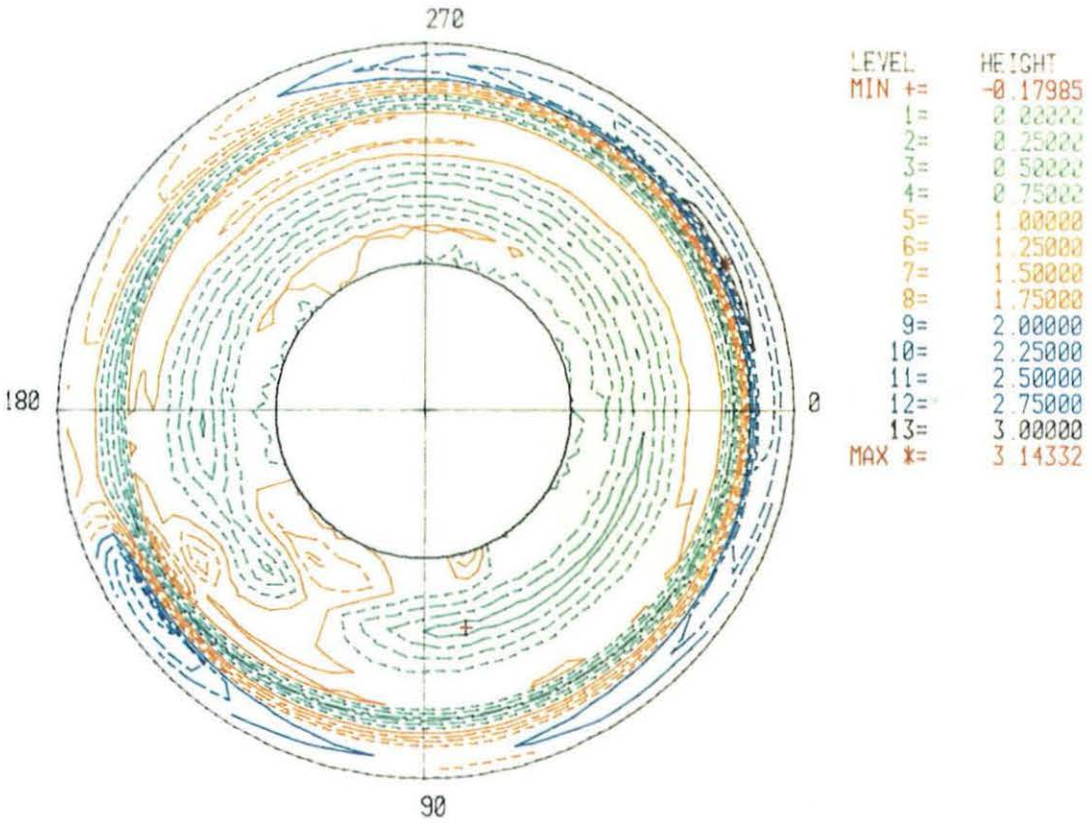

Fig 13. Polar plot of tail rotor negative Cp in hover

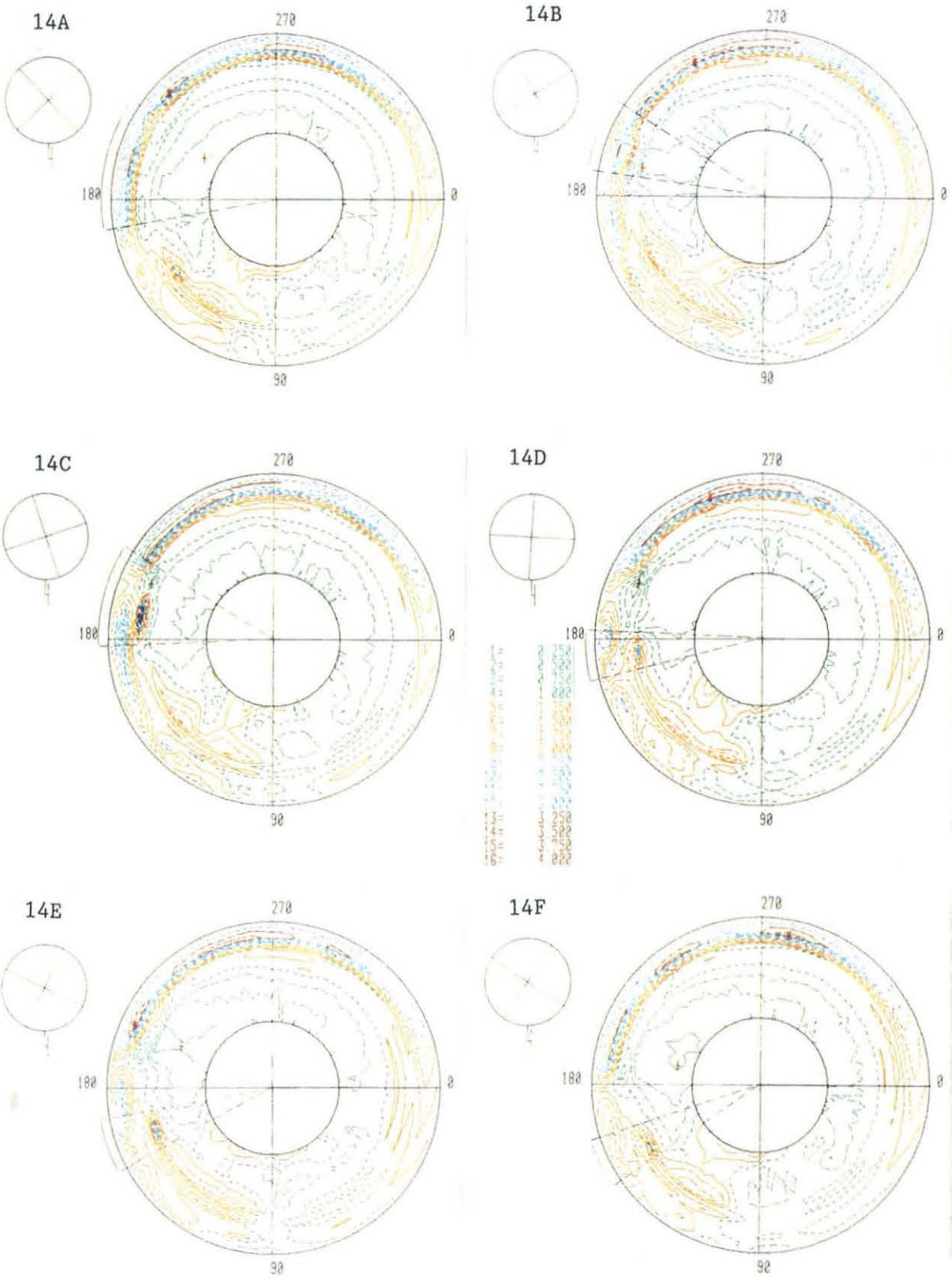

Fig 14. Polar plots of tail rotor negative Cp 10 Kts forward flight

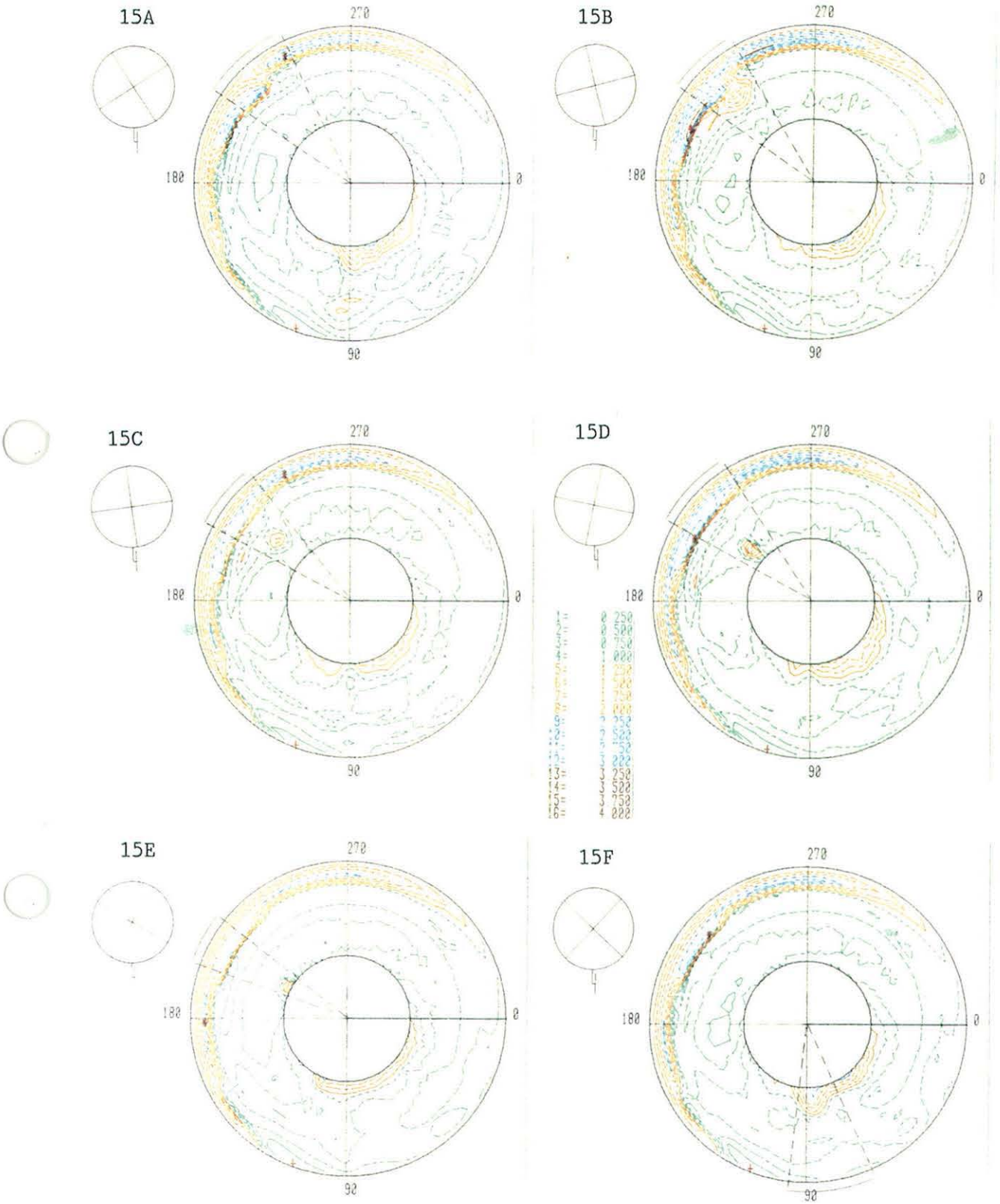

Fig 15. Polar plots of tail rotor negative Cp 20 Kts forward flight

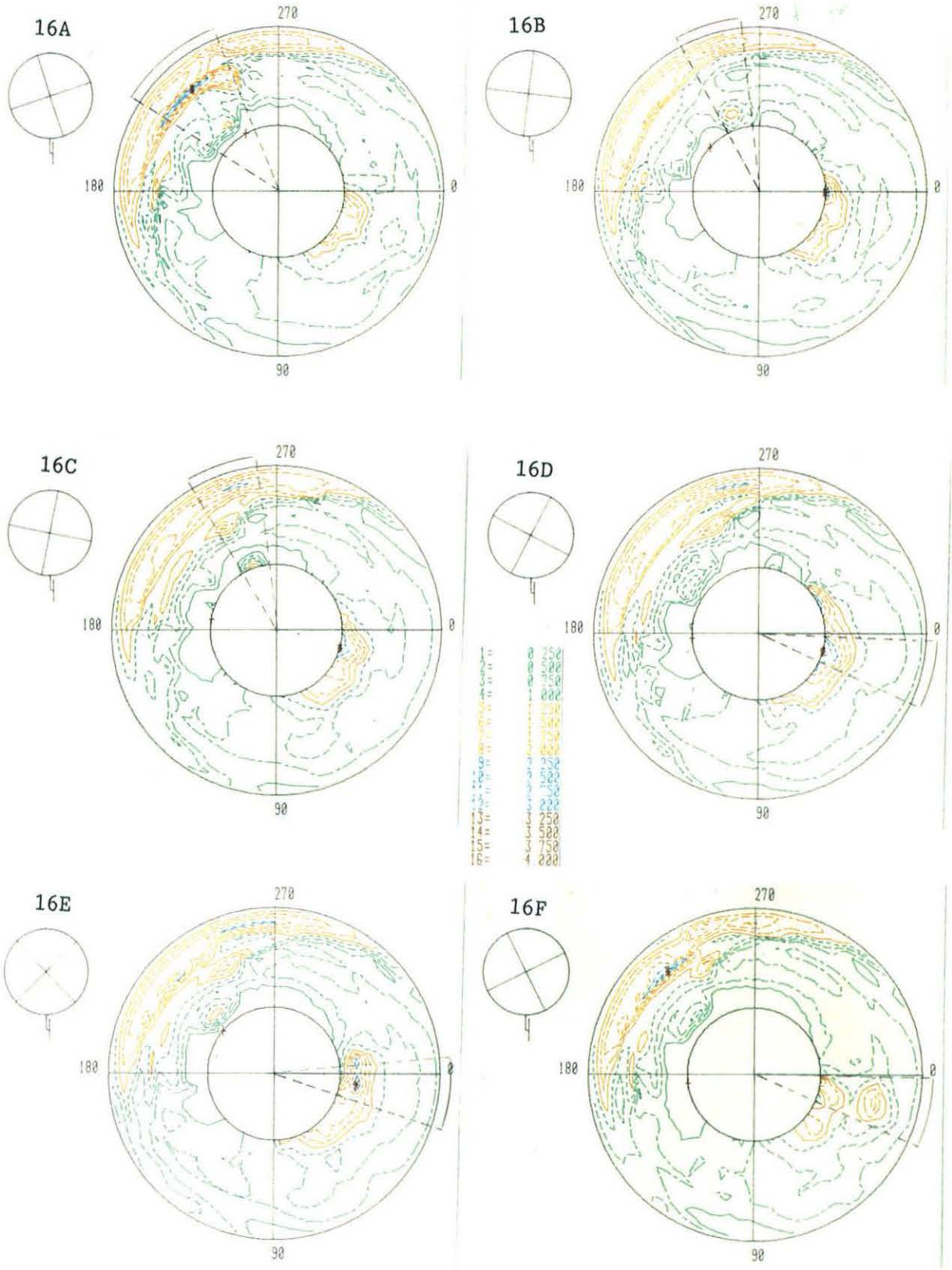

Fig 16. Polar plots of tail rotor negative Cp 30 Kts forward flight

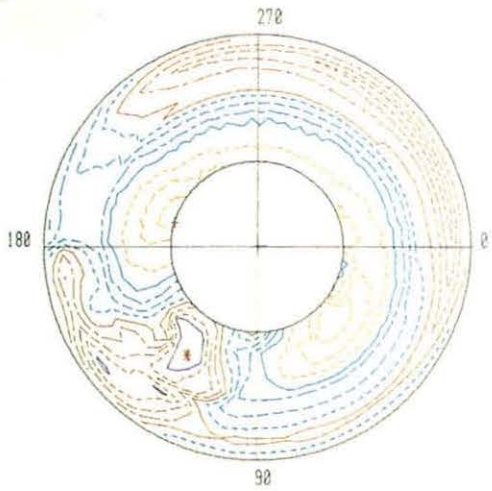

18A 10 Kts Red 90

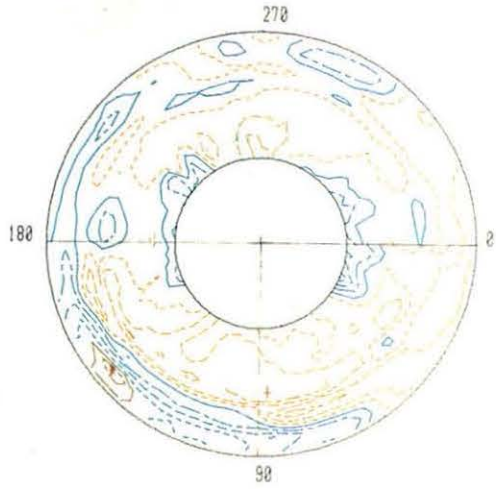

18B 10 Kts Green 75

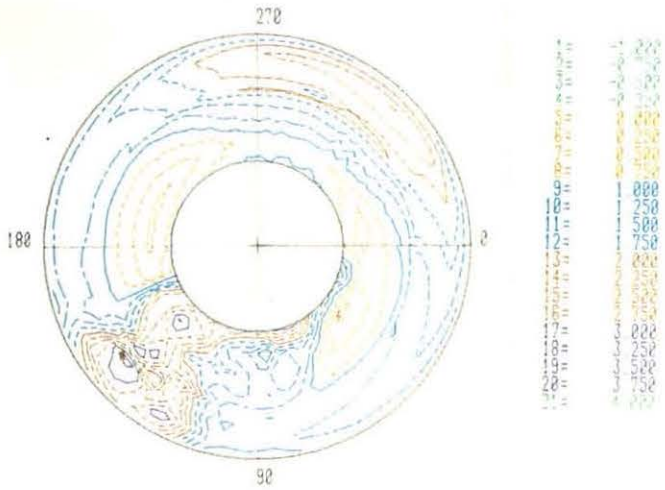

18C 20 Kts Red 95

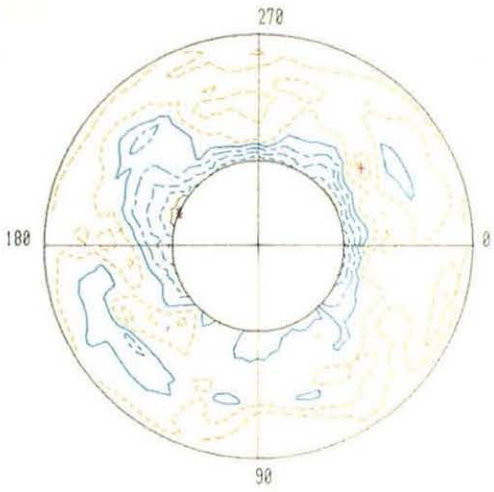

18D 20 Kts Green 90

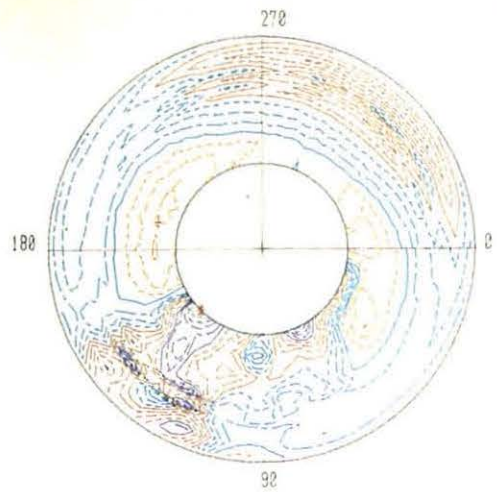

18E 30 Kts Red 95

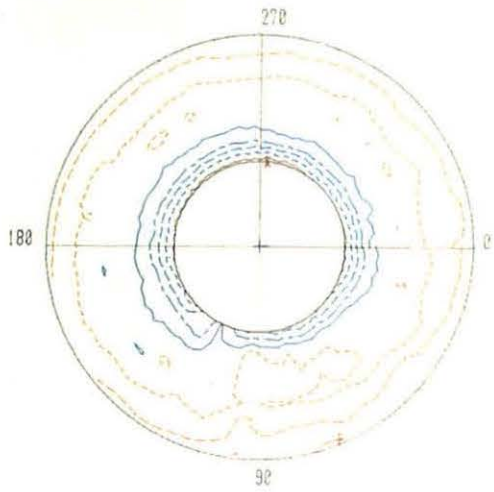

18F 30 Kts Green 90

Fig 18. Polar plots of tail rotor negative Cp in sideways flight